AIAA 2003-1062

On the Noise Generated by Convected Structures in a Mach 0.9, Hot, Turbulent Jet

F. P. Bertolotti

United Technologies Research Center, East Hartford, CT

Tim Colonius

Caltech, Pasadena, CA

41st Aerospace Sciences Meeting & Exhibit

January 6-9, 2003 / Reno, NV

On the noise generated by convected structures in a Mach 0.9, hot, turbulent jet

Fabio P. Bertolotti
United Technologies Research Center
411 Silver Lane, East Hartford, CT. 06108

Tim Colonius
Division of Engineering and Applied Science
California Institute of Technology
Pasadena, CA 91125

* Abstract

Solutions to the linearized equations of motion are used to study sound radiation by convected disturbances in the jet core. The spectrum of eigenmodes reveals the presence of modes that represent convected vortical and entropic motions in the potential core of the jet. We investigate the near-field acoustics produced by these core modes using the Parabolozied Stability Equations. At the conditions of commercial jet engines during take-off, the core modes radiate sound effectively along Mach lines due to the jet centerline velocity being supersonic relative to the fee-stream speed of sound. Summing three of these modes to create two distinct disturbances – one that is velocity dominated, and another that is entropy dominated – one observes that entropy variations radiate sound more effectively than vortical variations.

The results yield a first insight into the impact of large-scale mixing inhomogeneities on the acoustic field. Such disturbances are created by devices in the jet engine itself, such as flow mixers, turbine exit vanes, and combustion-chamber (i.e. pattern factors).

1 Introduction

Our analytical study focuses exclusively on a high Reynolds number, turbulent, Mach 0.9 jet with a core temperature of 708 K exiting into a co-flowing Mach 0.1 free-stream at ambient temperature and pressure. This overall flow is representative of the jets emitted by some of the current commercial jet engines during take-off or landing. The hot jet has a mean core velocity that is subsonic relative to the local sound speed but is supersonic relative to the sound speed in the far field. Consequently, unsteady vortical and entropic structures, such as those that constitute turbulence, convected in the core flow will radiate sound in an efficient manner as Mach waves.

Over the past 20 years, linear theory has been developed to predict the sound generated by instability waves with supersonic phase velocity. The development of matched asymptotic expansions (MAE), which expand the near-field solution of the linearized flow equations with the spreading rate as a small parameter and match this expansion to a global solution to the wave equation in the far field, have been developed for mixing layers[1] and jets[2]. The noise amplitude predicted by a linear theory is directly proportional to the amplitude of the fluctuations at the nozzle lip which are typically unknown. To predict noise, additional assumptions about the excitation of linear modes are required. For example, the stochastic wave model developed by Tam and Chen [3] considers a single instability wave at any given frequency as representative of the energy carrying wave component (that is, it neglects the continuous spectrum of convected disturbances). They argue that the instability wave spectrum of the jet may be regarded as being generated by the stochastic white noise excitation at the nozzle lip region. Thus the amplitude of instability waves are set by matching the turbulent kinetic energy of the flow at the nozzle lip. Using similar approaches, a vari-

ety of investigations of the noise from supersonic instability waves have now been performed for different jet conditions (e.g.[4, 5, 6]).

In contrast to previous studies that have focused on the sound produced by the onset and growth of "organized structures" within the shear layer, our study focuses on structures that are generated by events upstream of both the jet orifice and our computational domain, and are convected by the core flow for the entire length of the potential core. We refer to these convected disturbances as "core modes". Examples of upstream hardware generating core modes are combustors (e.g. the "pattern factor"), turbine exit guide vanes, fan-stream & jet-stream mixers, and flow turbulence in general Core modes can be separated into those dominated by vorticity, and those dominated by temperature variations (entropy).

Our primary investigative tool are the linearized Parabolized Stability Equations [7] [8], and both the linearization step and the parabolization step are better justified for the analysis of sound generation by the core modes than the sound generation by the shear-layer modes. The reasons for this are explained in section 2, below.

Working with linearized equations brings some advantages to our study, the most prominent of which is the ability to generate a complete spectrum of modes at any one axial location. Any small-amplitude motion in the jet, as well as outside of it can be expanded into a series of these modes [9], hence, by studying the sound radiated by each individual mode, we hope to gain a fundamental insight into the sound radiated by turbulence convecting in the core flow – an insight different from that gained using published methods based on statistical cross-correlation measurements and/or turbulence models.

The motivation for our work is an understanding of the process by which large-scale components of the turbulence field within the core of the jet and within the first six jet diameters generates sounds. Some specific questions include: are vortical modes louder than hot-spots (i.e.entropy modes?), does sound radiation efficiency diminish or increase at small scales? or at high frequencies?

Our study is exploratory in nature, and methods for comparing our results with experimental measurements still need to be defined.

2 Justification for the use of the linearized PSE

To justify our use of the PSE, two issues must be addressed: first, the use of linearized equations per se, and, second, the use of parabolized equations.

The use of the solutions to the linearized Navier-Stokes equations to model some aspects of decaying turbulence have been very successful in the past. (example: to model the response of a laminar boundary layer to free stream turbulence [10]). Both in the free-stream and in the jet's core, the mean flow is absent of shear – hence turbulence production – and most flow disturbances, including turbulence, simply convect and decay. The process of convection is exactly modeled by the linearized equations, so the only real issue is whether the decay rate displayed by the eigenmodes of the linearized solutions approximates sufficiently well the decay rate displayed by solutions to the full equations. Baring transient growth, which may be conceptually possible for some specific low-frequency motions, the effect of nonlinearity can be crudely estimated by comparing the magnitude of the nonlinear terms to the convective terms. At 10% turbulence levels this comparison yields a value of about 1%, hence we anticipate that eigenmodes of the linearized equations are well suited for our study.

The same conclusion cannot be reached for the shear-modes, since nonlinear phenomena – and in particular subharmonic instabilities – may play a key role in the sound generation process, as can be inferred by the occurrence of the peak in measured sound levels at Strouhal numbers below those predicted by linear theory. Moreover, direct comparisons of linear and nonlinear calculations of (cold) jets with the same inflow forcing have shown that the linear theory significantly underpredicts the noise radiation from the shear modes [11].

We now discuss the issue regarding parabolization of the equations. The linearized PSE are easily solvable equations for tracking the evolu-

tion of a single eigenmode in a flow with weakly non-parallel streamlines. The streamwise wavenumber α_e of the mode may (and usually does) change with streamwise distance x, and the PSE accurately track this change. If the mean-flow were perfectly parallel then α_e would be constant and a Fourier transform of the disturbance field would yield a single delta function at $\alpha = \alpha_e$. However, when the flow is non-parallel, α_e varies in x and a Fourier transform of the disturbance flow-field yields a Gaussian-like function that is centered at roughly the average value of $\alpha_e(x)$ and has a width that increases with increasing variation in α_e.

At each value of α where the function is non-zero we can compute a phase speed $c = \omega/\alpha$ (the frequency ω of the mode is constant) and, if the phase speed is supersonic relative to the sound speed a_∞ in the free-stream, there is sound radiation along a Mach line with angle dependent on α. If the phase speed is subsonic, there is no sound radiation. Thus, the value $\alpha_{acc} = \omega/a_\infty$ is the cut-off wavenumber, and only wavenumbers smaller than α_{acc} radiate sound.

Consider now a shear mode and a core mode in our particular flow. The shear mode travels subsonically with respect to a_∞ and has strong variation in α_e on account of the streamwise growth of the shear layer. A sketch of what the Fourier transform of this mode's flow field might look like is shown as curve "B" in figure 1. The peak of the function lies to the right of the cut-off wavenumber α_{acc}, hence most of the energy in the mode does not radiate sound, and only a small amount of energy at the left tail of the function extending past α_{acc} will cause sound radiation. Since the PSE track α_e and $\alpha_e > \alpha_{acc}$, there will be no sound radiation present in the PSE solution.

A sketch of what the Fourier transform of the core mode's flow field might look like is shown as curve "A" in figure 1. Since the core mode is convected at supersonic speeds, then $\alpha_e < \alpha_{acc}$ and essentially all the energy of the eigenmode is involved in sound radiation. The PSE solution now contains the generated sound field associated with the wavenumber α_e, but does not contain the sound radiated by wavenumbers significantly different from α_e. Thus, the acoustic field displayed by the PSE solution is incomplete. However, we do not need to calculate the radiation at all radiating wavenumbers to get some basic insight into the sound radiation process for a core mode, or to compare sound levels between different core modes. The PSE solution captures the sound generated at the most "energetic wavenumbers", and this suffices for our exploratory work – e.g. deductions about peak sound directivity and amplitude can be made. Refinements in the computation of the acoustic field can be made (e.g. [12]) and are part of our continuing work.

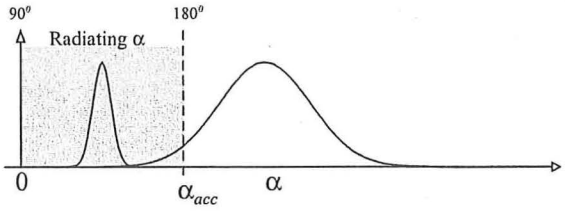

Figure 1: Sketch of wavenumber content of a supersonic and subsonic traveling modes.

3 The mean flow

The mean-flow for our stability analysis was furnished by an axis-symmetric Reynolds averaged Navier Stokes solution. We employed the WIND code from the NPARC alliance, using the Spalart-Allamaras turbulent model. A fine grid, employing 321 x 281 grid-points, was constructed using a differentiable mapping from numerical to physical space to improve the smoothness of the solution, but, due to our use of a highly accurate spectral multi-domain discretization of the stability equation, a small amount of smoothing was performed on the RANS solution.

In what follows, the nozzle exit diameter and jet centerline values at the nozzle exit are used for non-dimensionalizing all quantities. Specific reference quantities corresponding to the mean flow solutions are: $L = 0.08224$ m, $U_r = 471$ m/s, $T_r = 708$ K, $\rho_r = 0.495$ kg/m^3, $M = 0.9$. Pressure is normalized with the dynamic pressure $\rho_r U_r U_r = 109,811$ Pa. The conditions correspond to a model in use at UTRC's acoustic facilities.

Figure 2 shows the isolines of streamwise ve-

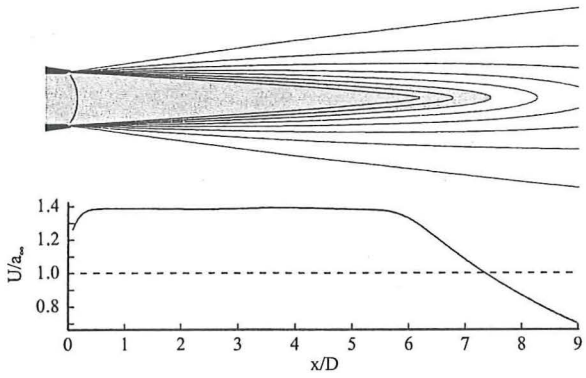

Figure 2: Streamwise velocity isolines of the mean-flow. Gray area denotes potential-core region having supersonic flow relative to free-stream sound speed. The lower plot shows the jet centerline velocity.

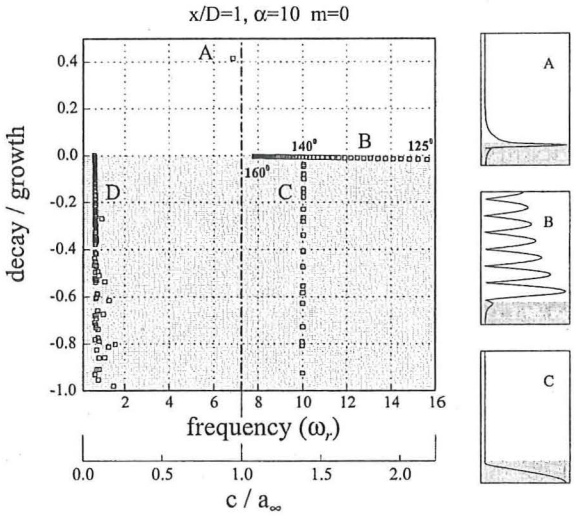

Figure 3: Temporal spectrum at $x = 1$, $\alpha_e = 10$ and $m = 0$. The additional horizontal axis shows the phase-speed c with respect to the free-stream sound speed.

locity on the upper plot, and the centerline velocity, nondimensionalized with the free-stream sound speed a_∞, in the lower plot. The gray color denotes the region in the flow where the flow is supersonic relative to a_∞.

4 The core modes

As noted in the introduction, linearized stability theory provides, at any chosen axial location, the spectrum of eigenvalues and associated eigenmodes which can be summed together to represent any possible small-amplitude disturbance in the flow. Herein, we describe the eigenmodes in detail.

Our disturbances have the form:

$$\mathbf{q}(x,r,\theta,t) = \hat{\mathbf{q}}(x,r)\, exp\left[i\,m\,\theta - i\,\omega\,t + \int_{x_0}^{x} \gamma_e(\xi) + i\alpha_e(\xi)\, d\xi \right] \quad (1)$$

where ω is the frequency, m is the azimuthal wavenumber, γ_e and α_e are the real and imaginary part of the streamwise wavenumber, and where the subscript e denotes "eigenmode". The axial location x_0 is the beginning of our computational domain, which starts at $x = 0.4$.

We solve the associated governing equations using a spectral multi-domain discretization in r 26 spectral domains are used, each with 15 Chebyshev polynomials per variable. In addition, the PSE employ a backward Euler in x. The computational domain extends from $x = 0.4$ to $x = 12$, and from the jet axis to $r = 25$.

A spectrum of disturbances at $x = 1$ is shown in figure 3. This spectrum was obtained by specifying the streamwise wavenumber of the disturbance $\gamma_e = 0$ $\alpha_e = 10$ and the azimuthal wavenumber $m = 0$, and computing the radian frequency ω as the eigenvalue. (This specification is opposite of that used in the PSE, wherein ω is specified and $\alpha_e(x)$ is solved for. Solving for ω as the eigenvalue is much simpler and less computationally intensive than solving for α_e as the eigenvalue).

The imaginary value of ω is shown on the vertical axis and determines the growth or decay of an eigenmode. The real value of ω is shown in the horizontal axis, and determines the frequency of the eigenmode. Since α_e is constant for this calculation, and since the phase-speed c of each eigenmode is given by the ratio ω/α_e, the frequency is proportional to the phase speed, hence the phase speed can be plotted as an additional axis in the figure. Due to our choice of reference velocity, the value $c = 1$ corresponds to the jet centerline velocity. The value of c corresponding to sonic velocity in the free-stream is $c = a_\infty = 0.71$.

Four families of modes appear in the spec-

trum, and are labeled A through D in the figure. Modes of type A correspond to the Kelvin-Helmholtz shear-layer instabilities, and are most energetic in the shear-layer region. One mode appears in our spectrum and is amplified in time (or space). This mode travels subsonically w.r.t. a_∞, hence this mode does not radiate sound energy directly along Mach lines, but, rather, radiates sound purely due to the flow non-parallelism, as discussed above.

Modes of type B are acoustic modes, and only exists at phase speeds greater than a_∞. The Mach-wave angle is simply related to the frequency, so that the directivity is 180 degrees (i.e. along the jet axis, downstream) when $c = a_\infty$, and decreases to 90 degrees as $\omega \to \infty$. The wavelength $2\pi/\delta$ of the sinusoidal variation of the eigenmode in the free stream is set by $\sqrt{\alpha_e^2 + \delta^2} = \omega/a_\infty$.

Eigenmodes C and D represent convected disturbances in the flow. This fact can be inferred from the plot by the equality in phase speed all the D modes. Modes of type C (i.e. core modes) have a phase speed of unity, showing that these modes are convected with the potential core of the jet. Modes D have a low phase-speed, corresponding to the free-stream velocity. Since both vortical and entropic disturbance are convected with the flow, and since the set of all eigenmodes forms a complete set [9], it follows that each mode of family C and D include either vortical or entropy variations or some combination of the two.

Since the domain outside the jet is unbounded, the modes of type "D" form a continuous spectrum. This spectrum appears discrete in the figure due to the necessarily finite-dimensional discretization of our numerical solution. The continuous spectrum can be parameterized by a real-valued scalar, e.g. arc length s, and to each value of s there corresponds a mode having a sinusoidal variation in the free-stream with wavenumber δ proportional to s.

In regards to the continuous versus discrete nature of the "C" mode spectrum, we note that the "C" eigenmodes have significant energy only within the core of the jet. In figure 4 we show the density and streamwise velocity variation for selected core modes, as well as the corresponding mean-flow value as a dashed line. We label

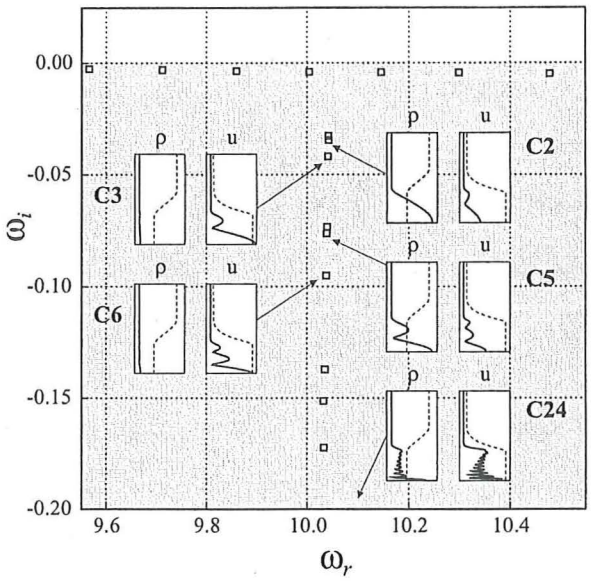

Figure 4: Eigenfunctions for selected core modes. The spectrum shown is a magnification of that in figure 3.

the core modes as "C1", "C2", "C3", etc, in order of appearance along the core-mode spectrum, starting from the least amplified. The labels remain unchanged as the frequency and azimuthal wavenumber are varied. These modes decay rapidly outside the potential core. A bounded support for the modes would imply that the "C" mode spectrum is discrete, rather than continuous, hence parameterized by a integer n. For each increasing n, at least one of the five components of the eigenmode (i.e. density, velocity and temperature) picks-up an extra maxima and minima in the profile. In figure 4, selected eigenmodes are shown along the "C" spectrum, and the increase in radial "wavenumber" is evident. The increase in damping with increase in n or radial wavenumber follows from the fact that modes with small scales decay faster than those with large scales. For example, for uniform mean-flow in Cartesian coordinates, the spatial decay rate as function of the three spatial wavenumbers α_e, δ and β (in x, y, and z) is given by ()

$$\gamma_e = \sqrt{\alpha_e^2 + \delta^2 + \beta^2}/R_0 \qquad (2)$$

where R_0 is the Reynolds number. An essentially similar equation exists for cylindrical coor-

dinates. Thus, we postulate that the core-mode spectrum spectrum ("C") is discrete (but infinite) at all Reynolds numbers, and becomes a true continuous spectrum only in the limit of an infinite Reynolds number. In the next sections, we investigate the efficiency of these modes in radiating sound.

5 The sound radiation from core modes

Our investigation into the effectiveness of sound radiation from core modes explores four parameters: (a) the effect of frequency (or, equivalently, spatial length scale), (b) the effect of azimuthal wavenumber, (c) the effect of location along the "C" spectrum, and, lastly, the effect of mode superposition to create velocity dominated motions and entropy dominated motions. This last case attempts to answer the question of which component of turbulence is more effective in radiating sound, vorticity or entropy (i.e. density and temperature hot-spots).

To compare sound intensities, all eigenmodes were normalized at the upstream end of the computational domain (i.e. $x = 0.4$) in the same manner. A normalization based on disturbance enthalpy was initially used but later discarded in favor of the normalization:

$$max\left(\hat{\rho}_{max}, \hat{u}_{max}, \hat{v}_{max}, \hat{w}_{max}, \hat{T}_{max}\right) = 1 \quad (3)$$

where the subscript max denotes the maximum along the radial coordinate r. This normalization will facilitate comparison with experimental data in the future.

Figure 5 shows the instantaneous sound fields (right) and associated amplitude fields (right) for a C1 mode with zero azimuthal number and various frequencies. The sound fields in this figure, as well as those in figure 5 and 5 have been multiplied by r to compensate for the attenuation of sound during propagation and, hence, better display the direction of sound propagation. We note that this normalization is consistent with a conical Mach wave, and removes the dominant decay that would be observed in the intermediate field. Further propagation would in reality yield spherical waves (decaying with $R = \sqrt{r^2 + x^2}$), but parabolization of the equations modifies this behavior. Moreover, as discussed above, the acoustic field computed from the PSE is not accurate near and after the end of the potential core, x = 6, so our acoustical field measurements are restricted to what is normally considered the near-field. However, as stated earlier, this limitation still allows an exploration into the sound generation process.

Strouhal	$\lvert p_{acc}\rvert$	$\lvert \mathbf{V}_{max}\rvert$	$\lvert \rho_{max}\rvert$	$\lvert T_{max}\rvert$
0.25	0.02400	1.0 (u)	0.528	0.541
0.50	0.01833	1.0 (u)	0.640	0.655
1.00	0.00506	1.0 (u)	0.720	0.738
1.50	0.00240	1.0 (u)	0.370	0.380

Table 1: Near-field peak acoustic pressure at a distance of 6 diameters from the nozzle. Core mode "C2" with $m = 0$ azimuthal wavenumber. Velocity, density and temperature maximums measured within the jet at $x = 1$.

The main sound directivity occurs along the Mach line, at roughly 140 degrees. At $x > 6$ the acoustic results are not complete, and some bending of the wavefront towards lower angles occurs at values of r and x ¿ 6, contrary to the change of the Mach-lines to lower angles at these locations. The most likely cause of this effect is the inaccuracy of the PSE approach to calculate the acoustic signal in the far field.

The peak values of the acoustic field along a locus of points at constant distance of 6 from the origin are reported in table 1. The acoustic energy is apparently a maximum at lower frequencies and decreases noticiably at frequency above St=0.5. The data shown can be used to calculate actual sound levels. For example, a St=0.5 mode with a velocity perturbation of 5% of U_r (i.e. 23 m/s), hence 3.275% of T_r (i.e. 23 K), will generate a peak acoustic pressure in the near field of $0.01833 \times 5\% \times 109811 = 100$ Pascal (SPL = 134 dB). . Since variations of about 5% in the velocity and temperature are quite likely in the exhaust of commercial engines, the core modes are apparently a significant sound source.

Figure 5 displays the effect of increasing azimuthal number. Maximum sound radiation occurs for the axis-symmetric mode (m=0) and decreases strongly with with increasing azimuthal number. Table 2 displays the maximum acous-

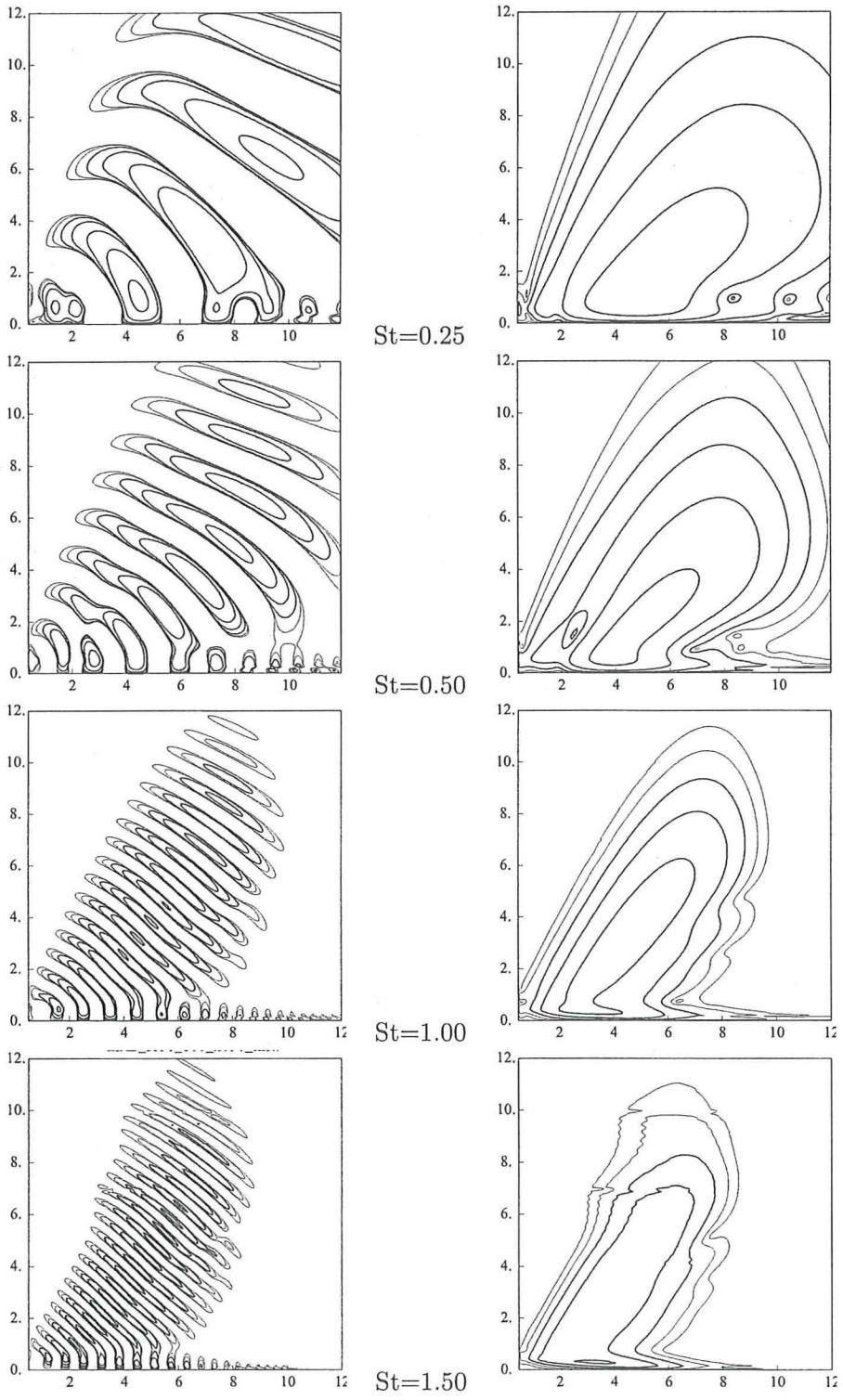

Figure 5: Positive iso-contours of pressure for Mode "C2" (m=0). Horizontal axis is x, vertical axis is r. Left column shows the instantaneous pressure multiplied by r, the right column shows the absolute value multiplied by r. "St" denotes Strouhal number. Contour levels at 1×10^{-4}, 3×10^{-4}, 0.001, 0.003, 0.01, 0.03, 0.1.

m	$\|p_{acc}\|$	$\|V_{max}\|$	$\|\rho_{max}\|$	$\|T_{max}\|$
0	0.01833	1.0 (u)	0.640	0.655
1	0.00272	1.0 (w)	0.440	0.280
2	0.00181	1.0 (v)	0.200	0.206
3	0.00035	1.0 (u)	0.220	0.230
4	0.00005	1.0 (u)	0.230	0.234
5	0.000005	1.0 (u)	0.250	0.260

Table 2: Near-field peak acoustic pressure at a distance of 6 diameters from the nozzle. Core mode "C2" with freqeuncy $St = 0.5$ and various azimuthal wavenumbers. Velocity, density and temperature maximums measured within the jet at $x = 1$.

tic pressure along a locus of points equidistant (6 units) from the nozzle exit, located outside the jet. The decrease is stronger than the decrease due to increasing frequency, although both higher frequency and azimuthal number yield smaller scales.

So far, we have focused on one of the least stable core modes. We now investigate the sound generation by different modes from the core-mode spectrum. Figure 5 compares the sound field generated by the C2, C3, C5 and C6 modes at Strouhal=0.50 and zero azimuthal number, and table 3 provides a summary. The sound amplitudes are comparable, suggesting that the "radial" wavenumber of the core modes has only a weak effect on the sound radiation.

6 Vortical vs. Entropic structures

We take advantage of the linearity of the governing equations to compare the relative efficiency of sound generation between convected structures that are vorticity dominated and structures that are density and temperature dominated.

For this study, we employ modes with Strouhal frequency of 0.5 and azimuthal wavenumber of 1. We construct a first structure with a dominant velocity field by summing the modes C1, C2, and C3 with weights chosen to minimize the amplitude of the density, temperature, and pressure fields. We then construct a second structure with dominant density and temperature fields relative to the velocity fields, also minimizig pressure. Pressure is minimized in both cases since convected disturbances are not accompanied by significant pressure variations. Figure 6 illustrates for each of the C1, C2, and C3 modes the variation of density, temperature, and three velocity components with r at an axial location of $x = 1$. To facilitate comparisons we have chosen the scaling such that the entropy and vorticity structures have maximum values of density (about 0.1) and velocity (about 1), respectively, that are similar to those of the C modes.

In figure 6 we show the same quantities for the velocity dominated and entropy dominated disturbances. While a complete elimination of velocity motions or density motions is not possible in our two structures, the difference is sufficient to produce strong differences in sound generation.

Table 4 displays the maximum acoustic pressure in the near field for each of the three modes C1, C2, and C3, and the density dominated and velocity dominated structures. The acoustic signal from the vortical mode is larger, 6.23×10^{-3}, compared with 2.36×10^{-3} for the entropy mode, however, if we take into account our scaling, the sound generated by the entropy mode is higher for equal % amplitude of density or velocity fields. For example, using the data from this table, we see that the entropy mode with just a 4% variation in temperature (i.e. 30 K) and, hence, 8% variation in velocity (37 m/s), yields an acoustic pressure of $(0.04/0.105) * 2.36 \times 10^{-3} * 109811 = 98$ Pa (SPL = 133 dB), while the vortical mode with a 8% variation in velocity yields 54 Pa (SPL = 128 dB). Knowing the actual amplitude of unsteady temperature and vortical stuctures emmitted by a jet engine would allow us to make a more definitve statement on the relative importance of these two types of structures.

7 Conclusion

This exploratory work uses solutions to the linearized equations of motion to study the fundamental mechanism by which disturbances in the jet core, produce and radiate sound. The results yield an insight into the sound generation mechanism of convected turbulence and large-

Mode	$\lvert p_{acc}\rvert$	$\lvert \mathbf{V}_{max}\rvert$	$\lvert \rho_{max}\rvert$	$\lvert T_{max}\rvert$
C2	0.01833	1.0 (u)	0.640	0.655
C3	0.00978	1.0 (w)	0.094	0.097
C5	0.00975	1.0 (v)	0.094	0.097
C6	0.01100	1.0 (u)	0.152	0.157

Table 3: Near-field peak acoustic pressure at a distance of 6 diameters from the nozzle, for a Strouhal = 0.5 mode with zero azimuthal wavenumber, $m = 0$. Velocity, density and temperature maximums measured within the jet at $x = 1$.

Mode	$\lvert p_{acc}\rvert$	$\lvert \mathbf{V}_{max}\rvert$	$\lvert \rho_{max}\rvert$	$\lvert T_{max}\rvert$
C1	5.46×10^{-3}	1.0 (w)	0.044	0.011
C2	3.10×10^{-3}	1.0 (w)	0.055	0.058
C3	4.16×10^{-3}	1.0 (w)	0.058	0.059
E	2.36×10^{-3}	0.26(u)	0.105	0.106
V	6.23×10^{-3}	1.0 (w)	0.014	0.014

Table 4: Near-field peak acoustic pressure at a distance of 6 diameters from the nozzle. Strouhal = 0.5, $m = 1$ azimuthal wavenumber. Modes C1, C2, C3, and entropy-dominated structure (E) and velocity dominated structure (V). Velocity, density and temperature maximums measured within the jet at $x = 1$.

scale mixing inhomogeneities created by devices in the jet engine itself.

The solutions to the Navier-Stokes equations linearized about a steady RANS solution for a Mach 0.9 hot jet display four types of motions, namely a Kelvin-Helmholtz shear-layer instability, acoustic modes, core modes representing vorticity and entropy convected within the potential core of the jet, and outer modes representing vorticity and entropy convected within the free-stream.

We used the Parabolozied Stability Equations to calculate the near-field acoustics produced by these modes. We find that the convected modes radiate sound effectively along Mach lines due to their supersonic phase speed (relative to the fee-stream speed of sound). The sound pressure level in the near-field is roughly 1 to 2 percent of the maximum velocity or temperature variations of the modes in the potential core. . The sound-pressure amplitude decreases with increasing azimuthal wavenumber, and increasing frequency, but is insensitive to the selection of core modes from the core-mode spectrum.

Summing three of these modes to create two distinct disturbance – one that is velocity dominated, and another that is entropy dominated – one observes that entropy variations radiate sound much more effectively than vortical variations. This suggests that even small radial variations in temperature in the core of the jet will radiate sound when the variations are unsteady in time.

We close by reiterating some limitations and extensions of our analysis that will be addressed in future work. First, the parabolization of the equations of motion has an impact on the radiated sound, although as we have discussed, the peak radiation at the Mach angle is correctly captured at relatively short propagation distances from the jet. This is sufficient to draw conclusions about the *relative* radiative efficiency of the convected core modes. However, it would be interesting to compare the radiation obtained by, say, using acoustic analogy with the same disturbance field, or by comparing a reference case with the full linearized Navier-Stokes equations (see, for example, Mohseni et al.[11]). Finally, a key question that remains is to what extent nonlinear PSE (e.g. [13]) could be used to predict the radiation from the shear (Kelvin-Helmholtz) modes? In the present jet these modes have subsonic phase speed and PSE alone cannot capture their radiation. However, combined with a suitable acoustic analogy, one could in principle compute the radiation.

8 References

References

[1] Tam, C. and Morris, P., "The radiation of sound by the instability waves of a compressible plane turbulent shear layer," *J. Fluid Mech.*, Vol. 98, 1980, pp. 349–381.

[2] Tam, C. and Burton, D., "Sound generation by instability waves of supersonic flows. Part 2. Axisymmetric jets," *J. Fluid Mech.*, Vol. 138, 1984, pp. 273–295.

[3] Tam, C. and Chen, P., "Turbulent mixing noise from supersonic jets," *AIAA J.*, Vol. 32, No. 9, 1994, pp. 1774–1780.

[4] Tam, C., Chen, P., and Seiner, J., "Relationship between instability waves and noise of high-speed jets," *AIAA J.*, Vol. 30, No. 7, 1992, pp. 1747–1752.

[5] Dahl, M. and Morris, P., "Noise from supersonic coaxial jets. 1. Mean flow predictions," *J. Sound Vib.*, Vol. 200, No. 5, 1997, pp. 643–663.

[6] Dahl, M. and Papamoschou, D., "Analytical predictions and measurements of the noise radiated from supersonic coaxial jets," *AIAA J.*, Vol. 38, No. 4, 2000, pp. 584–591.

[7] Bertolotti, F. P., Herbert, Th., and Spalart, P. R., "Linear and nonlinear stability of the Blasius boundary layer," *J. Fluid Mech.*, Vol. 242, 1992, pp. 441–474.

[8] Herbert, Th., "Parabolized Stability Equations," *Ann. Rev. Fluid Mech.*, Vol. 29, 1997, pp. 245–283.

[9] Grosch, C. E. and Salwen, H., "The continuous spectrum of the Orr-Sommerfeld equation. Part 1. The spectrum and the eigenfunctions," *J. Fluid Mech.*, Vol. 87, 1978, pp. 33–54.

[10] Bertolotti, F.P., "Response of the Blasius boundary layer to free-stream vorticity," *Phys. Fluids A*, Vol. 9, No. 8, 1997, pp. 2286–2299.

[11] Mohseni, K., Colonius, T., and Freund, J., "An evaluation of linear instability waves as sources of sound in a supersonic turbulent jet," *Phys. Fluids*, Vol. 14, No. 10, 2002, pp. 3593–3600.

[12] Balakumar, P., "Prediction of supersonic jet noise," *AIAA Paper 98-1057*, 1998.

[13] Day, M., Mansour, N., and Reynolds, W., "Nonlinear stability and structure of compressible reacting mixing layers," *J. Fluid Mec.*, Vol. 446, 2001, pp. 375–408.

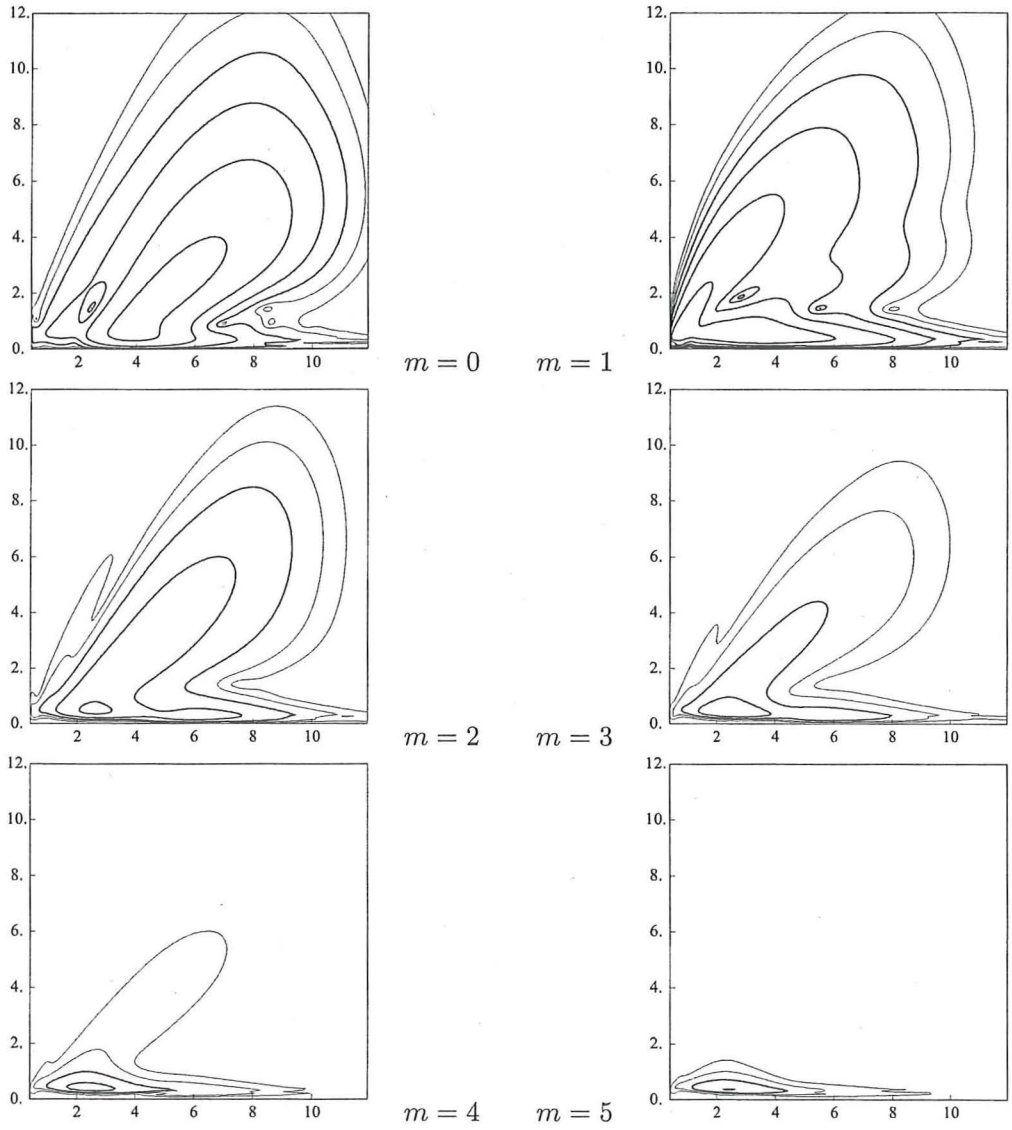

Figure 6: Iso-contours of $|p|$ for Mode "C2" at a Strouhal number of 0.5 and various azimuthal numbers. Horizontal axis is x, vertical axis is r. Contour levels at 1×10^{-4}, 3×10^{-4}, 0.001, 0.003, 0.01, 0.03, 0.1.

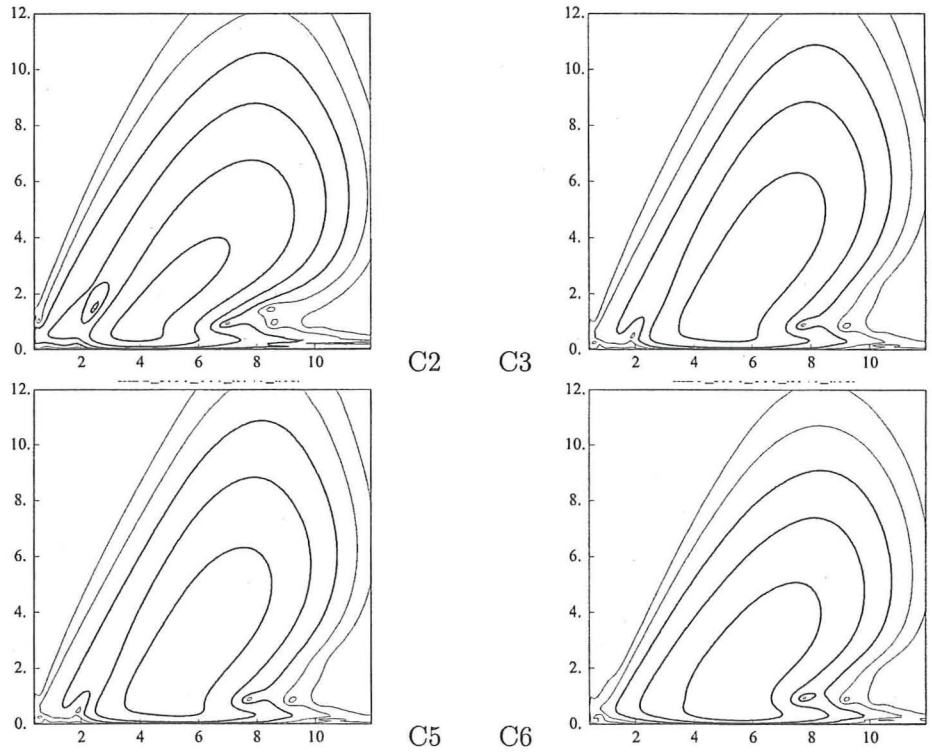

Figure 7: Iso-contours of $|p|$ for various core modes at a Strouhal number of 0.5 and zero azimuthal number. Horizontal axis is x, vertical axis is r. Contour levels at 1×10^{-4}, 3×10^{-4}, 0.001, 0.003, 0.01, 0.03, 0.1.

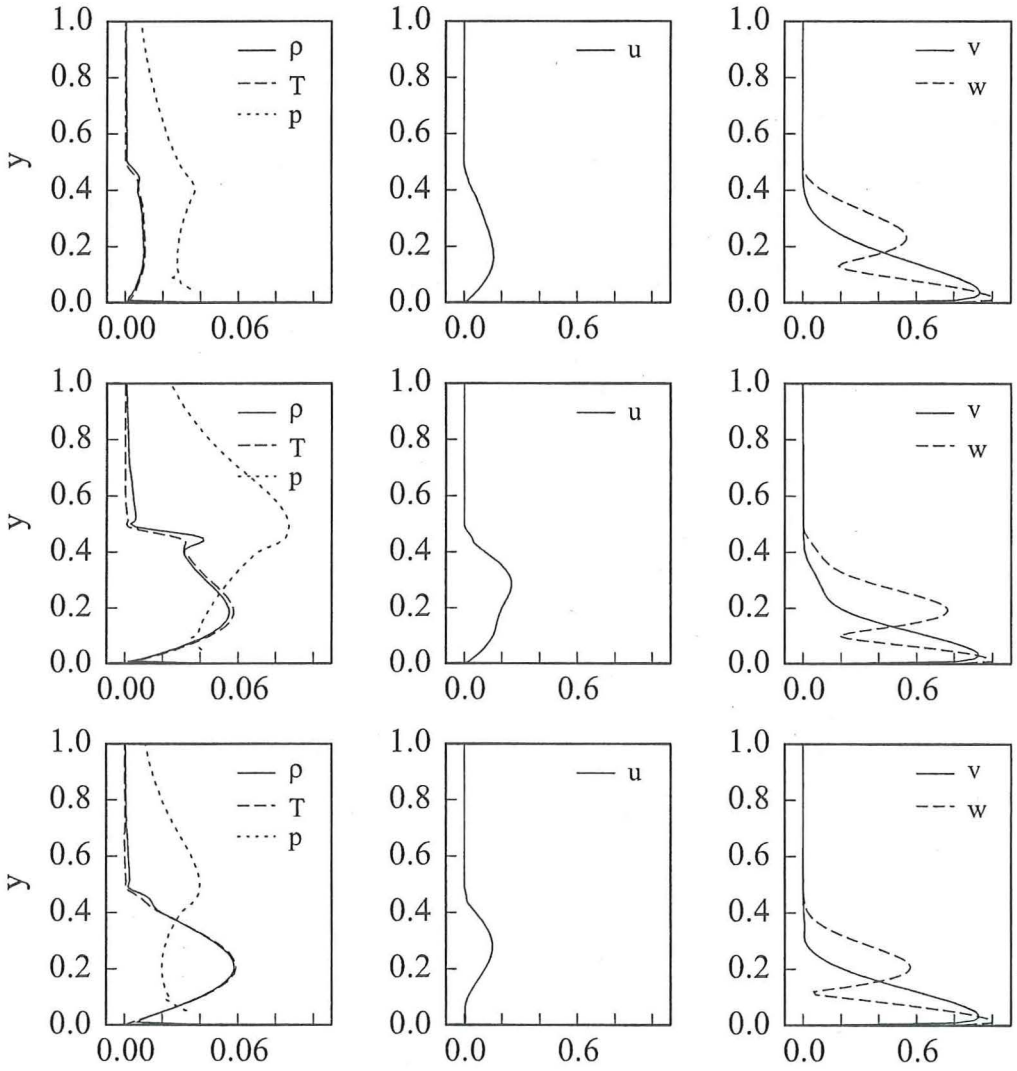

Figure 8: Radial profiles at $x = 1$ of the C1, C2, and C3 eigenmodes at a Strouhal number of 0.5 and $m = 1$ azimuthal number.

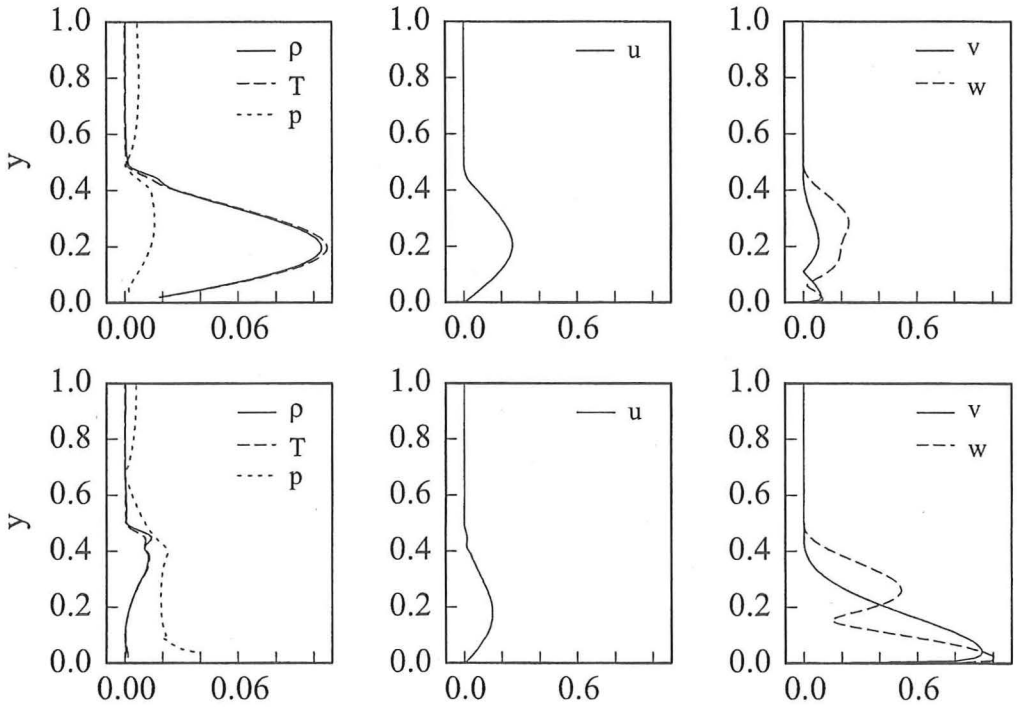

Figure 9: Radial profiles at $x = 1$ of the density dominated structure (above) and velocity dominated (below). Strouhal number 0.5 and $m = 1$ azimuthal number.